2023 Volume 1, Issue 2
Computer Simulation in Application
ISSN: 2630-4597 (Online)

Computer Simulation-Assisted Preparation and Application of Triadimenol Molecularly Imprinted Polymer

Guodong Li[1], Lianpeng Jing[1], Zengliang Li[1], Xuyu Tang[1], Lili Gu[1]*, Junli Shi[2], Jieyun Cai[3]

[1]College of Chemical Engineering, Kunming University of Science and Technology, Kunming 650500, China

[2]Yunnan Tobacco Agricultural Science Research Institute, Yuxi 653100, China

[3]Yunnan Tobacco Quality Supervision and Testing Station, Kunming 650106, China

***Corresponding author:** Lili Gu, liligu001@163.com

Abstract:

Computer simulation technology was employed to design the pre-polymerization system for triadimenol (TDM) molecularly imprinted polymer. The optimal functional monomer identified was methacrylic acid (MAA), and the molar ratio of TDM to MAA (TDM-MAA) was established as 1:3 for the pre-polymerization process. Thermodynamic analysis indicated that the TDM-MAA self-assembly was a non-spontaneous, endothermic reaction, with a suitable pre-polymerization reaction temperature of 30℃. Leveraging the computer simulation results, triadimenol molecularly imprinted polymer nanoparticles (TDM-MIPs) with a uniform particle size distribution and a large specific surface area were synthesized via precipitation polymerization. These TDM-MIPs exhibited adsorption affinity for TDM and its structural analogs. The molecularly imprinted polymer was then utilized as a solid-phase extraction filler to fabricate a molecularly imprinted solid-phase extraction (MISPE) column for the pretreatment of tobacco leaf samples. Ultra-high performance liquid chromatography-tandem mass spectrometry (UPLC-MS/MS) was subsequently employed to detect and analyze the pretreated tobacco leaf extracts. The average recovery rates for the four triazole fungicides ranged from 88.3% to 100.68%, with relative standard deviations (RSDs) of 2.9% to 9.3%. Consequently, a TDM-MISPE-UPLC-MS/MS method was established for the simultaneous detection of trace levels of triadimenol, triadimefon, myclobutanil, and tebuconazole in tobacco leaves.

Keywords:

Computer simulation
Molecularly imprinted polymer
Adsorption
Triadimenol
Solid phase extraction

Online publication: December 22, 2023

1. Introduction

Triadimenol (TDM) is a common triazole fungicide used in agricultural production [1]. Due to its stable nature and resistance to degradation, TDM can persist for long periods in crops and their growing environments [2,3], making it crucial to monitor TDM residues in agricultural products.

Currently, detection methods for triazole fungicides primarily include gas chromatography [4], high-performance liquid chromatography (HPLC) [5], gas chromatography-mass spectrometry (GC-MS) [6], and ultra-high performance liquid chromatography-tandem mass spectrometry (UPLC-MS/MS) [7]. To ensure the reliability of test results, samples require pretreatment before detection to minimize matrix effects that may interfere with the analysis. Molecular imprinting technology (MIT) refers to a technique that uses imprinted molecules as templates to prepare and utilize molecularly imprinted polymers (MIPs) with specific recognition capabilities for the imprinted molecules [8]. MIPs prepared based on this technology are characterized by their specific recognition ability, high selectivity, good stability, and long service life, making MITs widely used in research fields such as chromatographic analysis, solid-phase extraction, and bionic sensors [9,10].

In recent years, with the development of computer technology and quantum chemistry, the use of computer software to assist in the design of molecular imprinting polymerization systems has been reported [11,12]. Li *et al.* [13] determined, based on density functional theory (DFT), that the optimal functional monomer for forming hydrogen bonds with triadimefon (TDF) is methacrylic acid (MAA), and the optimal molar ratio of template to monomer is 1:4. Guided by this, the imprinting factor of TDF-MIPs prepared via precipitation polymerization reached 2.42. Hou *et al.* [14] screened suitable functional monomers and solvents for magnetic MIPs through DFT, reducing the preparation cycle of magnetic molecularly imprinted membranes. In this study, DFT was used to predict the TDM-MIPs polymerization system, screen the optimal functional monomer, and determine the ratio of template molecules to functional monomers. Guided by computer simulation results, TDM-MIPs were prepared using acetonitrile [13], a solvent suitable for precipitation polymerization. The adsorption performance and application in solid-phase extraction (SPE) of TDM-MIPs were explored, and a MISPE-UPLC-MS/MS method was established for the simultaneous detection of trace amounts of TDM and its analogs in tobacco leaves.

2. Materials and methods

2.1. Instruments and reagents

Tecnai G2 TF30 S Twin scanning electron microscope (SEM, FEI Company, Netherlands); Zetasizer Nano ZS90 Malvern particle size analyzer (Malvern Instruments, USA); Equinox55 Fourier transform infrared spectrometer (FTIR, Bruker Corporation, Germany); Agilent 1290 Infinity UHPLC ultra-high performance liquid chromatograph (Agilent Technologies, USA); AB Sciex Qtrap (TM) 3200 MS/MS mass spectrometer (AB Sciex, USA); Simulation optimization software (Gaussian 09, Gaussian Inc., USA). TDM (purity 99%), tebuconazole (TEB, purity 98%), simetryn (SMT, purity 99%), atrazine (ATZ, purity 99%) (Dr. Ehrenstorfer GmbH, Germany); TDF (purity 99%), myclobutanil (DMT, purity 98.5%) (Aladdin Reagent Company); azobisisobutyronitrile (AIBN, AR), ethylene glycol dimethacrylate (EGDMA, AR) (Beijing Bailingwei Technology Co., Ltd.).

2.2. Experimental methods

2.2.1. Computer simulation of triazole molecular imprinting pre-assembly system

Using DFT, the complex conformations, binding energies, and intensity distributions of five functional monomers with TDM were simulated and calculated via Gaussian 09 software. The polymerization ratios of different functional monomers with TDM were inferred. Further thermodynamic analysis of the self-assembly process was conducted to determine the suitable temperature for the self-assembly process. The infrared spectra of the template-monomer complexes in vacuum and acetonitrile were simulated and compared with actual infrared spectra. The calculation steps are as follows: (1) Optimize the geometric conformations of the template molecule and functional monomers at the B3LYP/6-31G+(d, p) level, and predict their active sites based on electrostatic potential distribution; (2) Perform energy calculations on the template-monomer complexes at the WB97XD/def2tzvp level to screen out the best functional monomer

and determine the optimal molar ratio of template to monomer; (3) Calculate the vibrational frequencies of the complexes in vacuum and acetonitrile at the WB97XD/def2tzvp level to obtain infrared spectra of the complexes. Estimate the pre-polymerization temperature through thermodynamic analysis of the complexes.

2.2.2. Preparation of TDM molecularly imprinted nanospheres

A total of 0.1 mmol TDM, 0.3 mmol MAA, and 25 mL acetonitrile were sequentially added into a 100 mL borosilicate glass bottle. The mixture was sonicated to achieve uniform mixing and purged with N_2 for 15 minutes to remove O_2. Pre-polymerization was carried out at 30°C for 12 hours. Following pre-polymerization, 20 mg AIBN and 2 mmol EGDMA were added, and the mixture was purged with N_2 for another 15 minutes. Thermal polymerization was then conducted at 60°C for 24 hours. After polymerization, the mixture was cooled to room temperature, centrifuged at 10,000 r/min for 10 minutes, and the supernatant was discarded. The resulting solid was dried to constant weight in a vacuum drying oven. The dried polymer was placed in a Soxhlet extractor and eluted using a methanol-acetic acid (9:1, V/V) mixture until no TDM was detected in the supernatant. The polymer was washed with methanol until it reached neutrality and dried at 40°C to constant weight, yielding the TDM-MIPs. For the control, non-molecularly imprinted polymers (NIPs) were prepared using the same steps as the TDM-MIPs, except no template molecules were added.

2.2.3. Dynamic adsorption

Each of 0.01 g TDM-MIPs and NIPs was weighed into 10 mL centrifuge tubes. To each tube, 4 mL of 50 μmol/L TDM-acetonitrile solution was added. Adsorption was allowed to occur at 25°C for 15, 30, 45, 60, 90, 120, and 150 minutes, respectively. The mixtures were centrifuged at 8,000 r/min for 10 minutes, and 2 mL of the supernatant was taken and filtered through a 0.22 μm membrane for UPLC-MS/MS detection.

2.2.4. Static adsorption

Each of 0.01 g TDM-MIPs and NIPs was weighed into 10 mL centrifuge tubes. To each tube, 4 mL of TDM-acetonitrile solutions with different concentrations (0.15, 0.3, 1.5, 3, 15, 30, 40, 50 μmol/L) were added. Adsorption was conducted at 25°C for 60 minutes. The mixtures were centrifuged at 8,000 r/min for 10 minutes, and 2 mL of the supernatant was taken and filtered through a 0.22 μm membrane for UPLC-MS/MS detection.

2.2.5. Selective adsorption

Each of 0.01 g TDM-MIPs and NIPs was weighed into 10 mL centrifuge tubes. To each tube, 4 mL of acetonitrile solution containing different pesticides at a concentration of 3 μmol/L was added. Adsorption was carried out for 60 minutes at 25°C. The mixtures were centrifuged at 8,000 r/min for 10 minutes, and 2 mL of the supernatant was taken and filtered through a 0.22 μm membrane for UPLC-MS/MS detection.

3. Results and discussion

3.1. Computer simulation of the triazole molecularly imprinted pre-assembly system

3.1.1. Optimization of template molecule and functional monomer configuration

The geometric configurations and electrostatic potential distributions of the template molecule TDM and five functional monomers (acrylic acid (AA), acrylamide (AM), methacrylic acid (MAA), trifluoromethacrylic acid (TF-MAA), and 4-vinylpyridine (4-VP)) are shown in **Figure 1**. Based on the electrostatic potential distribution, it can be seen that TDM has two electron-accepting and one electron-donating position, while MAA, AM, and AA each have one electron-donating and one electron-accepting position. TFMAA has one electron-accepting position, and 4-VP has only one electron-donating position. In **Figure 1**, (1) red areas indicate electronegativity, and (2) blue areas indicate electropositivity. The deeper the color, the stronger the electronegativity or electropositivity, and the stronger the ability to accept or donate electrons. The positions with stronger electron donation and acceptance are also the most likely to form hydrogen bonds, thus allowing for initial judgment of the hydrogen bond binding positions and ratios between TDM and the functional monomers.

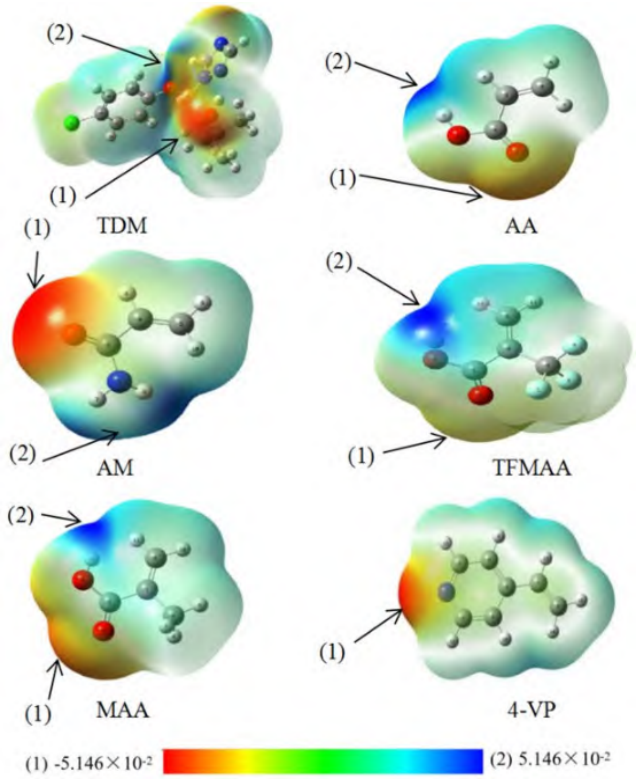

Figure 1. Electrostatic potential diagrams of TDM and functional monomers (AA, AM, TFMAA, MAA, 4-VP)

3.1.2. Selection of functional monomers

Figure 2 shows the optimized configurations of TDM and functional monomer complexes. There are four types of bonds between TDM and the functional monomers: O-HO, O-HN, N-HO, and N-HC. TDM binds with 4-VP via N-HC hydrogen bonding, but the bond length is not within the typical hydrogen bond length range (1.627~2.169 Å) [13], indicating that TDM and 4-VP cannot form a hydrogen bond. From the electrostatic potential distribution of TDM and the functional monomers in **Figure 1**, it can be observed that TDM can form up to three hydrogen bonds with AA, MAA, TFMAA, and AM. However, the hydrogen bond lengths formed between the 7H on AM's amino group and the 6N and 2O on TDM's triazole ring are 2.752 Å and 2.654 Å, respectively. The O-HN bond length between TDM and TFMAA is 2.663 Å, and the O-HN bond length between TDM and AA is 2.762 Å, all of which are outside the typical bond length range. Therefore, the molar ratio of TDM to AM is 1:1, the molar ratios of TDM to TFMAA and AA are both 1:2, and the molar ratio of TDM to MAA is 1:3. **Table 1** presents the hydrogen bond binding energies between TDM and the four functional monomers. The binding energy between TDM and MAA is the highest, followed by TFMAA, AA, and AM. A larger binding energy (|ΔE|) between TDM and the functional monomer indicates a stronger interaction, resulting in higher selectivity and affinity of the polymer imprint cavity. Therefore, MAA is the preferred functional monomer for preparing triazole molecularly imprinted polymers, and its molar ratio with TDM is 1:3.

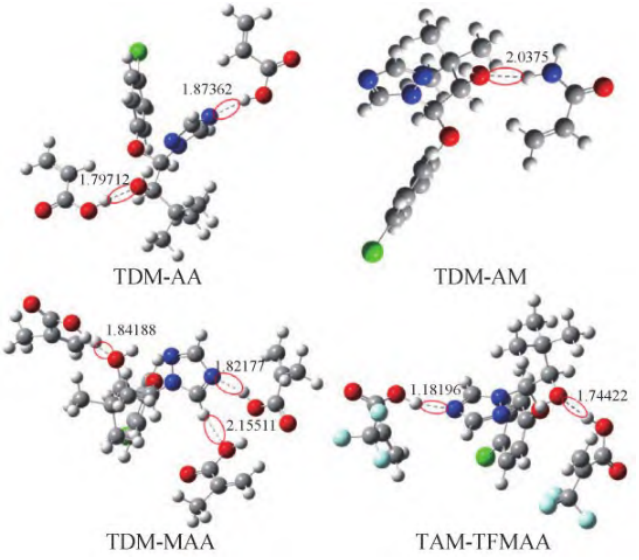

Figure 2. Composite structures of TDM recombined with four functional monomers

Table 1. Number of hydrogen bonds existed between TDM and four monomers and pre-polymerization interaction energy of ΔE

Composite	|ΔE|/(kJ/mol)	Number of hydrogen bond	Ratio
TDM-AA	98.47	2	1:2
TDM-MAA	137.98	3	1:3
TDM-TFMAA	117.44	2	1:2
TDM-AM	38.36	1	1:1

3.1.3. Thermodynamic process analysis of pre-polymerization

To better interpret the polymerization reaction (TDM+3MAA→Polymer) from a macro perspective, a thermodynamic analysis was conducted. The trends of enthalpy, free energy, and entropy changes during the TDM-MAA pre-polymerization were estimated in

Table 2. Thermodynamic data of pre-polymerization reaction at different conditions

Temperature/K	Vacuum			Acetonitrile		
	ΔH /(kJ/mol)	ΔG /(kJ/mol)	ΔS /(J/(mol/K))	ΔH /(kJ/mol)	ΔG /(kJ/mol)	ΔS /(J/(mol/K))
273.15	16.03	149.68	-0.495	14.42	146.76	-0.484
283.15	16.41	154.57	-0.488	14.80	151.59	-0.483
293.15	16.79	159.45	-0.487	15.18	156.41	-0.481
303.15	17.17	164.31	-0.485	15.56	161.23	-0.480
313.15	17.56	169.15	-0.484	15.95	165.96	-0.479

vacuum and acetonitrile media at temperatures ranging from 273.15 to 313.15 K. As shown in **Table 2**, during the pre-polymerization reaction, ΔH>0, ΔG>0, and ΔS<0. All three parameters increase with rising temperature, but the increase is relatively small. This indicates that the TDM-MAA pre-polymerization process is an endothermic and non-spontaneous reaction that is not significantly affected by temperature. To ensure sufficient pre-polymer formation, subsequent pre-polymerizations were conducted at 30°C.

3.1.4. Infrared spectroscopy analysis

Figure 3a shows the simulated infrared spectra (FTIR) of the TDM-MAA complex in vacuum and acetonitrile, while **Figure 3b** displays the actual prepared polymer's infrared spectrum. The main absorption peaks of the three infrared spectra lines are basically consistent, indicating that acetonitrile as a solvent has little effect on polymer synthesis. This also confirms the reliability of the simulated FTIR spectroscopy results, allowing for convenient and rapid determination of chemical bonds

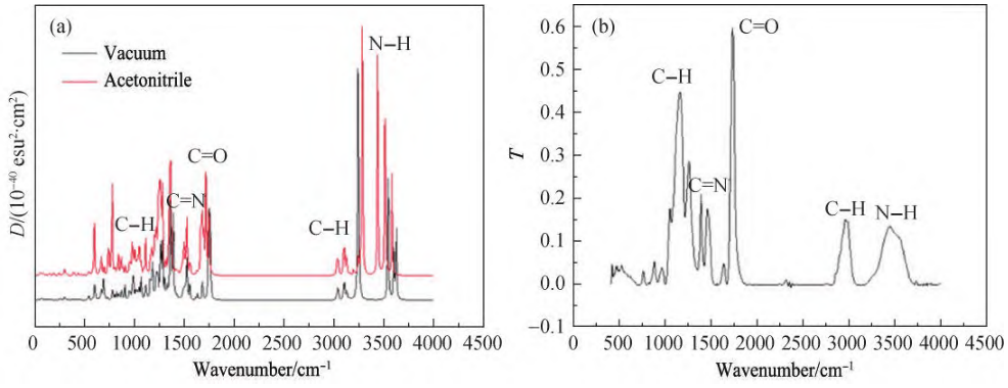

Figure 3. Infrared spectra of TDM-MAA in different media environment (a) and actual TDM-MAA (b)

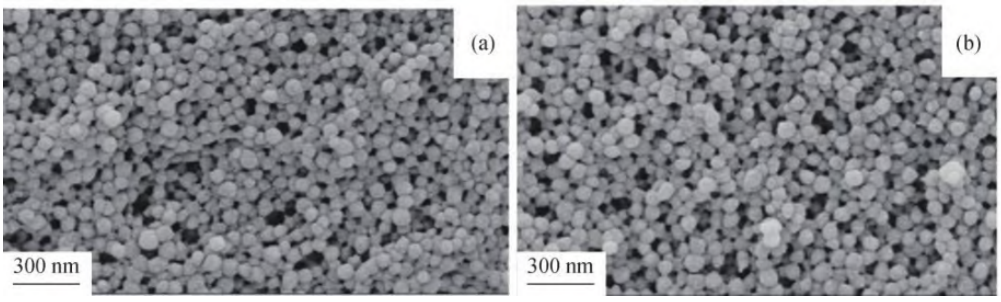

Figure 4. FE-SEM images of (a) MIPs and (b) NIPs

peak positions for the main groups in each segment. The presence of a C-OH carboxyl stretching vibration peak at a wavenumber of 1258 cm^{-1} indicates the existence of MAA in both MIPs and NIPs. All four spectra display a strong and sharp O-C-O stretching vibration peak at 1154 cm^{-1}, suggesting the presence of the crosslinking agent EGDMA. The sharp vibration peak near 1732 cm^{-1} is caused by the presence of C=O, indicating that a copolymerization reaction has occurred between the crosslinking agent EGDMA and the functional monomer MAA during the polymerization process. TDM and MIPs before elution show a C-Cl stretching vibration peak at 666.06 cm^{-1}, which is absent in the spectra of MIPs and NIPs after elution, confirming the complete removal of the template molecule TDM. In summary, the presence of EGDMA and MAA in the polymers is demonstrated, and the polymerization reaction between the template molecule, functional monomer, and crosslinking agent has occurred.

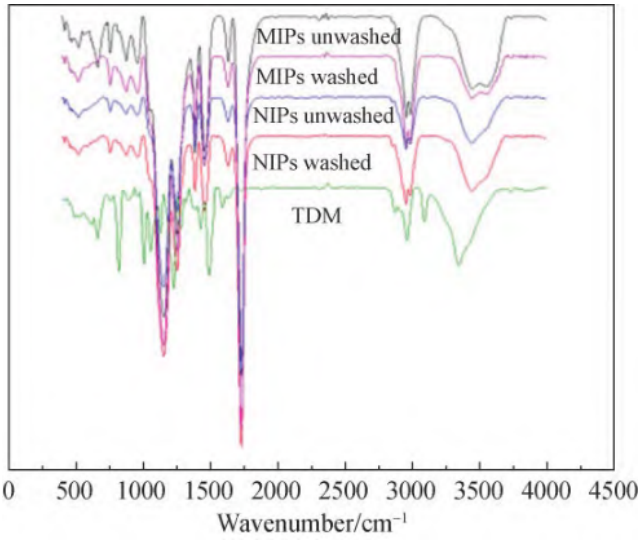

Figure 5. The FTIR spectra of washed and unwashed TDM-MIPs, NIPs, and TDM

3.3. Analysis of polymer adsorption properties

3.3.1. Dynamic adsorption performance and model analysis

The saturated adsorption properties of MIPs and NIPs were studied by varying the adsorption time to obtain the optimal equilibrium adsorption time for the polymers. The adsorption capacity, Q, was calculated using formula (1) [14]:

$$Q = (c_0 - c) \times V / m \quad (1)$$

Where Q represents the equilibrium adsorption capacity of the polymer for triazole alcohol (μg/g), c_0 denotes the concentration of the TDM-acetonitrile solution before adsorption (mg/L), c represents the concentration of the TDM-acetonitrile solution after adsorption (mg/L), V is the volume of the adsorption solution (L), m is the mass of the polymer (g).

Figure 6 shows the dynamic adsorption curves for MIPs and NIPs. The adsorption capacity of the polymers for triazole alcohol increased rapidly with increasing adsorption time and stabilized after 60 minutes. The adsorption capacity of MIPs was always higher than that of NIPs within the same time frame. This is because MIPs have a large number of specific adsorption sites on their surface, resulting in stronger adsorption capabilities, while NIPs only exhibit non-specific adsorption with weaker adsorption abilities. After 60 minutes, the adsorption of target molecules by specific adsorption sites was almost complete, and the adsorption of MIPs reached saturation. The adsorption and desorption amounts were roughly balanced, indicating that the polymers had reached adsorption equilibrium. Therefore, the subsequent adsorption time was selected as 60 minutes.

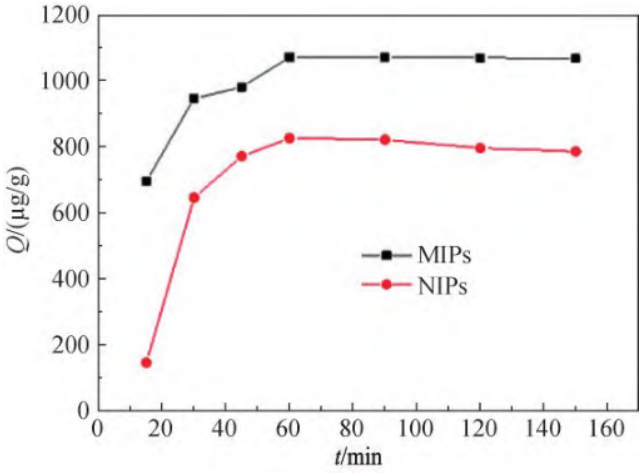

Figure 6. Dynamic adsorption curves of MIPs and NIPs

The dynamic adsorption process is analyzed using pseudo-first-order and pseudo-second-order adsorption models. The calculation formulas for these two kinetic adsorption models are given as (2) and (3) in reference [15]:

$$\log(Q_e - Q_t) = \log Q_1 - \frac{k_1}{2.303} \quad (2)$$

$$\frac{t}{Q_t} = \frac{1}{k_2 \times Q_2^2} + \frac{t}{Q_2} \quad (3)$$

In these equations, Q_e represents the equilibrium adsorption capacity of TDM-MIPs for TDM molecules (μg/g); Q_t represents the actual adsorption capacity of TDM-MIPs at time t (μg/g); Q_1 , Q_2 represent the theoretical adsorption capacities of TDM-MIPs in the pseudo-first-order and pseudo-second-order kinetic adsorption models (μg/g), respectively; k_1 , k_2 represent the adsorption equilibrium constants of TDM-MIPs in the pseudo-first-order and pseudo-second-order kinetic adsorption models g/(μg·min), respectively.

Figures 7a and **7b** show the pseudo-first-order and pseudo-second-order kinetic adsorption models, respectively. By comparing the linear fitting equations of the two kinetic adsorption models, it can be seen that the dynamic adsorption behavior of TDM-MIPs is more consistent with the pseudo-second-order kinetic model. At 60 minutes, the theoretical adsorption capacity Q_t is 1111.1 μg/g, which is very close to the actual adsorption capacity of $Q_{60\ min}$ = 1072 μg/g.

3.3.2. Static adsorption performance and Scatchard analysis

The adsorption performance of TDM-MIPs for different concentrations of TDM solutions was tested, and the binding site characteristics were analyzed using the Scatchard model to further derive the relationship between adsorption capacity (Q) and dissociation constant (K_d) [16].

The calculation formula for the Scatchard model is as follows (4):

$$\frac{Q}{c} = \frac{(Q_{Max} - Q)}{K_d} \quad (4)$$

In this equation, Q represents the equilibrium adsorption capacity of the polymer for TDM (μg/g); Q_{max} represents the maximum adsorption capacity of the TDM-MIPs adsorption sites (μg/g); c represents the equilibrium concentration of the TDM-acetonitrile solution (mg/L); K_d represents the equilibrium dissociation constant of the adsorption sites (mg/L).

Figure 8a shows the isothermal adsorption curves of TDM-MIPs and NIPs for static adsorption. It can be seen that the adsorption capacity of MIPs and NIPs for TDM increases with increasing TDM-acetonitrile solution

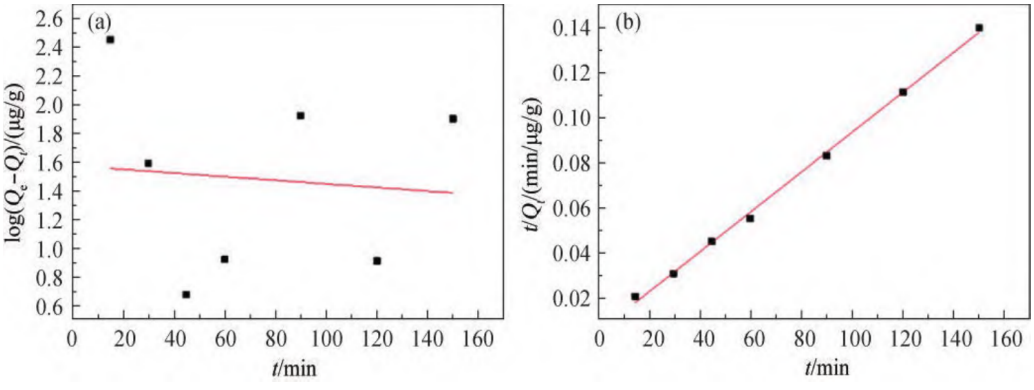

Figure 7. Kinetic quasi (a) first order reaction and (b) second order reaction models of TDM-MIPs

concentration. Comparing the isothermal adsorption curves of TDM-MIPs and NIPs, the adsorption capacity of MIPs is always higher than that of NIPs. This is because MIPs mainly adsorb TDM specifically, while NIPs only adsorb TDM non-specifically on the surface.

Figure 8b shows the Scatchard model analysis of the adsorption performance of TDM-MIPs. Based on the adsorption results of the polymer in the static adsorption experiment, a plot of Q/c versus Q is made for linear fitting. From **Figure 8b**, it can be seen that there are two linear fitting curves, indicating that TDM-MIPs have two types of adsorption sites for TDM: high and low. The dissociation constant for the high adsorption site is 19.17 μg/mL, and the maximum apparent binding capacity is 2249.15 μg/g. The dissociation constant for the low adsorption site is 0.58 μg/mL, and the maximum apparent binding capacity is 157.599 μg/g.

3.3.3. Selective adsorption

Figure 9 shows the adsorption capacities of TDM-MIPs and NIPs for six pesticides. It is evident that TDM-MIPs have stronger adsorption capabilities for triazole fungicides than for triazine herbicides, and the adsorption capabilities of MIPs are stronger than those of NIPs. This is because TDM, TEB, TMT, and TDF have similar structures, all containing a triazine ring. The specific cavity structure and adsorption sites in TDM-MIPs effectively adsorb target substances with similar structures, indicating that the MIPs have specific recognition capabilities, while NIPs only have physical surface adsorption. Triazine herbicides have significant structural differences from triazole fungicides, and TDM-MIPs do not specifically adsorb SMT and ATZ.

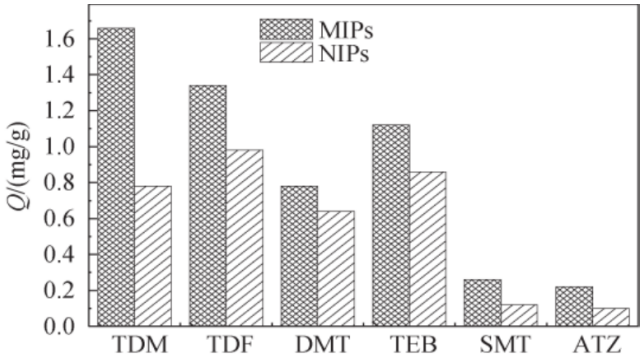

Figure 9. Selective adsorption of TDM-MIPs

3.4. Application of TDM-MIPs

3.4.1. Standard curve and detection limit

The four triazole fungicide pesticides exhibit a good linear relationship within the concentration range of 0.02 to 5 mg/L. The detection limit, determined using a signal-to-noise ratio (S/N) of 3 or higher, ranges from 2.21 to 3.32 ng/mL, as shown in **Table 3**.

3.4.2. Recovery rate and precision

Blank tobacco leaves were taken, and tobacco leaf extracts were prepared at three spiking levels: 0.2, 1, and 2 μg/g. These extracts were then pretreated with MISPE followed by detection using UPLC-MS/MS. The MISPE pretreatment effectively removes interference from the tobacco leaf matrix, enhancing the accuracy of detection. The recovery rate and relative standard deviation (RSD) were calculated, and the results are presented in **Table 4**. The average recovery rate of spiking ranged from 88.3% to 100.68%, with an RSD range of 2.9% to 9.3%. The adsorption performance and selective adsorption effect of TDM-MIPs for triazole fungicides are generally consistent.

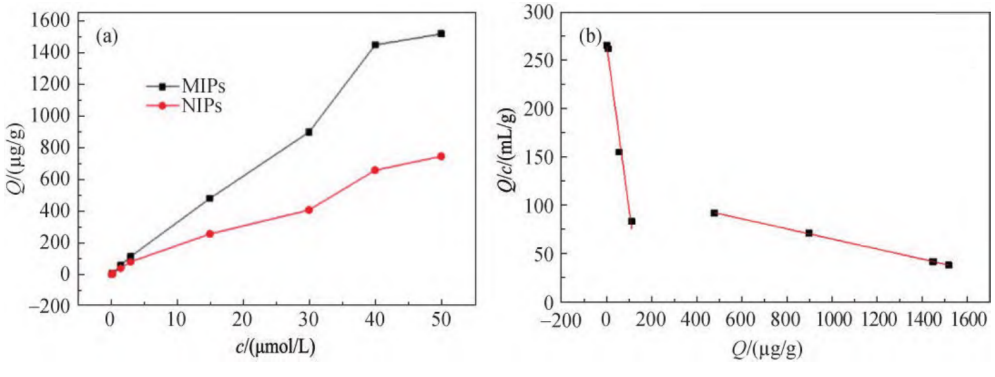

Figure 8. (a) Isotherms absorption curves of TDM-MIPs and NIPs; (b) Scatchard analysis of TDM-MIPs

Table 3. Standard curves, linear ranges, correlation coefficients and limits of detection (LODs) of four pesticides

Compound	Standard curve	Linear range/(mg/L)	R^2	LOD/(ng/mL)
TDM	y = 2360000x + 6560	0.02-5	0.9992	2.21
TDF	y = 1610000x + 243000	0.02-5	0.9941	3.32
DMT	y = 1980000x + 304000	0.02-5	0.9905	3.14
TEB	y = 3940000x + 114000	0.02-5	0.9911	2.62

Table 4. Spiked recoveries and RSDs after MISPE (n = 3)

Compound	Added/(μg/g)	Recovery/%	RSD/%
TDM	2	102.6	7.9
	1	103.0	4.9
	0.2	96.5	2.9
TDF	2	93.5	8.7
	1	89.2	7.8
	0.2	86.6	3.3
DMT	2	87.1	6.8
	1	86.3	4.7
	0.2	85.3	5.5
TEB	2	90.9	5.4
	1	87.2	3.8
	0.2	86.9	9.3

4. Conclusion

Based on Density Functional Theory (DFT), Gaussian09 software was employed to screen the optimal functional monomer, methacrylic acid (MAA), for the TDM-MIPs polymerization system. The infrared spectra of the TDM-MAA pre-polymerization process in acetonitrile and vacuum media were calculated. From a thermodynamic perspective, the pre-polymerization process was found to be non-spontaneous and endothermic, with a pre-polymerization temperature of 30℃. Using TDM as the template, MAA as the functional monomer, EGDMA as the cross-linker, AIBN as the initiator, and acetonitrile as the porogen, TDM-MIPs nanospheres were prepared via precipitation polymerization. These nanospheres demonstrated excellent specific recognition capabilities for TDM, with a saturated adsorption capacity reaching 1072 μg/g. The TDM-MIPs were utilized as solid-phase extraction fillers to prepare TDM-MISPE columns, establishing a method for simultaneous detection of four triazole fungicides in tobacco leaves using TDM-MISPE-HPLC-MS/MS. The results indicated that, after pretreatment with TDM-MIPs-MISPE and detection by UHPLC-MS/MS, the average recovery rates of the four triazole fungicides ranged from 88.3% to 100.7%, with RSD values of 2.9% to 9.3% (n = 3) and detection limits of 2.21 to 3.32 ng/mL.

Funding

Science and Technology Plan Project of China National Tobacco Corporation Yunnan Company (2017YN11, 2021530000241009)

Disclosure statement

The authors declare no conflict of interest.

References

[1] Zhao LW, Zhang L, Liu FM, et al., 2014, Multiresidue Analysis of 16 Pesticides in Jujube Using Gas Chromatography and Mass Spectrometry with Multiwalled Carbon Nanotubes as a Sorbent. J Sep Sci, 37(22): 3362–3369.

[2] Borucka M, Celiński M, Sałasińska K, et al., 2020, Identification of Volatile and Semi-Volatile Organic Compounds Emitted During Thermal Degradation and Combustion of Triadimenol. J Therm Anal Calorim, 139(2): 1493–1506.

[3] Wang ZK, Tian Z, Chen L, et al., 2020, Stereoselective Metabolism and Potential Adverse Effects of Chiral Fungicide Triadimenol on Eremias argus. Environ Sci Pollut Res, (27): 7823–7834.

[4] Farajzadeh MA, Afshar MMR, 2016, Acid–Base Reaction-Based Dispersive Liquid–Liquid Microextraction Method for Extraction of Three Classes of Pesticides from Fruit Juice Samples. J Chromatogr A, 1431: 8–16.

[5] Yi XT, Liu C, Liu XK, et al., 2019, Magnetic Partially Carbonized Cellulose Nanocrystal-Based Magnetic Solid Phase Extraction for the Analysis of Triazine and Triazole Pesticides in Water. Microchim Acta, 12(186): 825.

[6] André CV, Mariane GS, Eduardo CF, 2017, Solid-Phase Extraction of Triazole Fungicides from Water Samples Using Disks Impregnated with Carbon Nanotubes Followed by GC-MS Analysis. Int J Environ Anal Chem, 97(1): 29–41.

[7] Ma SP, Yuan XC, Zhao PF, et al., 2017, Trace Determination of Five Triazole Fungicide Residues in Traditional Chinese Medicine Samples by Dispersive Solid-Phase Extraction Combined with Ultrasound-Assisted Dispersive Liquid–Liquid Microextraction and UHPLC–MS/MS. J Sep Sci, 40(16): 3257–3266.

[8] Nazia T, Shahjadi K, Boris BD, 2020, Perspective and Application of Molecular Imprinting Approach for Antibiotic Detection in Food and Environmental Samples: A Critical Review. Food Control, 118: 107381.

[9] Sayyed HH, Massoud K, Ahmad JK, et al., 2020, Application of Molecularly Imprinted Polymer Pipette Tip Micro-Solid Phase Extraction of Nalidixic Acid and Acetaminophen from Pills and Seawater Samples and Their Determination by Spectrophotometry. Chem Pap, 74(11): 4009–4023.

[10] Parisa J, Ameneh PDS, 2020, A Novel Electrochemical Sensor Based on Molecularly Imprinted Polymer for Selective Determination of Tramadol in Biological Samples. J Anal Chem, 75(9): 1108–1116.

[11] Han Y, Gu LL, Zhang MX, et al., 2017, Computer-Aided Design of Molecularly Imprinted Polymers for the Selective Recognition of Triazine Herbicides. J Theor Comput Chem, 1121: 29–34.

[12] Li ZY, Gu LL, Tong ZH, et al., 2021, Computer Simulation Assisted Preparation and Application of Myclobutanil Imprinted Nanoparticles. Polymer, 217: 123457.

[13] Li ZY, Li ZJ, Gu LL, et al., 2020, Preparation and Application of Triazolone Molecularly Imprinted Nano-Spheres. Chemical Industry and Engineering Progress, 39(7): 2706–2714.

[14] Hou LM, Han XQ, Wang N, 2020, High Performance of Molecularly Imprinted Polymer for the Selective Adsorption of Erythromycin in Water. Colloid Poly Sci, 298(8): 1023–1033.

[15] Zhao XB, Pei WJ, Guo RL, et al., 2020, Selective Adsorption and Purification of the Acteoside in Cistanche tubulosa by Molecularly Imprinted Polymers. Front Chem, 7: 903.

[16] Zhang YH, Zhu YP, Loo LS, et al., 2021, Synthesizing Molecularly Imprinted Polymer Beads for the Purification of Vitamin E. Particuology, 57: 10–18.